Ductile Void Growing in Micromorphic GLPD Porous Plastic Solids Containing two Populations of Cavities with Different Sizes

Roy Burson and Koffi Enakousta

Abstract Gologanu, Leblond, Perrin, and Devaux (GLPD) developed a constitutive model for ductile fracture for porous metals based on generalized continuum mechanics assumptions. The model predicted with high accuracy ductile fracture process in porous metals subjected to several complex loads. The GLDP model performances over its competitors has attracted the attention of several authors who explored additional capabilities of the model. This paper provides analytical solutions for the problem of a porous hollow sphere subjected to hydrostatic loadings, the matrix of the hollow sphere obeying the GLPD model. The exact solution for the expressions of the stress and the generalized stress the GLPD model involved are illustrated for the case where the matrix material does not contain any voids. The results show that the singularities obtained in the stress distribution with the local Gurson model are smoothed out, as expected with any generalized continuum model. The paper also presents some elements of the analytical solution for the case where the matrix is porous and obeys the full GLPD model at the initial time when the porosity is fixed. The later analytical solution can serve to predict the mechanisms of ductile fracture in porous ductile solids with two populations of cavities with different sizes.

Keywords: Gradient Model · Analytical Solutions · Plasticity · Hollow Sphere Problem · Fracture

1 Introduction

Metal structures often fail by ductile rupture when they are subjected to external static or dynamic forces. The requirement to develop constitutive models (whether they are physics, mechanics and/or mathematics based) that can predict precisely ductile fracture processes in metals has become a key point in metal structure design community. So far, such community has widely accepted that the model proposed by [20] and extended by [32, 33] to account for cavities interactions and coalescence (these features were disregarded in [20]'s original work) following an earlier suggestion by [27] can adequately describes ductile fracture in metals.

R. Burson and
Department of Mathematics, California State University, Northridge, 18111 Nordhoff Street, Northridge, CA 91330
e-mail: Roy.burson.618@my.csun.edu

K. Enakousta
Department of Mathematics, California State University, Northridge, 18111 Nordhoff Street, Northridge, CA 91330 and Department of Mathematics, UCLA, Los Angeles, 520 Portola Plaza, Los Angeles, CA, 90095

Several extensions have followed these pioneering works; among them, let us mention the contributions of [23], [22], and recently [26]. The latter has modified Gurson model to include shear failure which often occurs, for instance, during high velocity impact failures of many steel.

Another modification of Gurson model including a characteristic length scale aimed at eliminating the pathological post-bifurcation mesh dependence issues proposed by [21] based on a previous suggestion of [24] in the context of concrete damage was adopted by [29, 28]. This proposal was studied in details by [8, 11] and adopted (thanks to its successes) in the context of high rate deformation and failure of materials by [12], [13], and [1]. However, the proposal was of less satisfaction from a theoretical and physical view points since it does not rely on any serious physical justification. This was the motivation of the development by Gologanu, Leblond, Perrin, and Devaux [19] of a second-gradient micromorphic model[1] for porous plastic materials. The GLPD model was obtained from a refinement of [20]'s original homogenization procedure, which was based on conditions of homogeneous boundary strain rate.

In contrast, the boundary velocity in the GLPD model approach was assumed to be a quadratic, rather than linear, function of the coordinates. The physical idea behind this assumption was to account in this way for possible quick variations of the macroscopic strain rate over very short distances, for example at the scale of the elementary cell the GLPD model is based on. The output of the procedure was a model of "micromorphic" nature, involving the second gradient of the macroscopic velocity and generalized macroscopic stresses of "moment" type (homogeneous to the product of a stress and a distance.) Other type of higher-order gradient models involing third-rank stress tensor with applications in bone remodeling design and other domain of interest exist. Among them let us mention the works by [31, 7, 5].

In practice, the GLPD model was extensively studied by [8, 18] who have notably shown that the model has the ability to predict mesh-independent FE solutions and to reproduce satisfactorily ductile fracture tests. Other numerical simulations involving second gradient models are available in the literature, see for instance [2, 30, 25]. A recent modification of the GLPD model numerical implementation developed in [8, 18] was suggested by [3] and yielded the same conclusions. The assessment of the reliability and accuracy of these two algorithms requires the development of analytical solutions that have served as critical cross references, see [8, 9, 15]. These solutions are based on two crude approximations so as for analytical solutions to be amenable: the porosity in the matrix material of the geometry considered was assumed to vanish.

The objective of the present paper is two-fold: (i) follow up the study of applications of the GLPD model to simple problems that might be of interest to validate the numerical implementation of this model into a finite element code and (ii) use the mechanical fields found to model cracking mechanisms in porous ductile solids containing two populations of cavities. The problem considered here is a hollow sphere subjected to a hydrostatic tension and made of a porous plastic material, obeying the GLPD model. We found the analytic solution of the hollow sphere problem in terms of deformation, stress and moment distributions under the conditions that the matrix obeys a reduced GLPD model for the case where the porosity vanishes. Also, we consider some elements of the solution of the problem in the presence of porosity in the matrix material, which is a rather complex type of problem. The complexity of the latter problem (a highly non-linear type of problem) forces us to present only some elements of the analytical solution at the initial time when the porosity is held constant. The rest of the paper is structured as follows:

- The first section describes the problem model, a hollow sphere subjected to an hydrostatic loading, the matrix obeying the GLPD model.

[1] micromorphic model will simply be denoted by GLPD model for shortness.

- Next, we assess the solution obtained for the case where the porosity vanishes. An algorithm that simulates the behavior of this model and analyzes the effects of the characteristic length scale on the distribution of stress and moments is also presented.
- In the section that follows, we consider the solution of the problem for the case where the porosity does not vanish at the initial time. We provide implicit analytic expressions for the Cauchy stress and moment components based on a highly non-linear ordinary differential equation, which involves the characterstic length scale of the GLPD model. Using then the associated flow rule we calculate the radial velocity. Employing the evolution law for the porosity we then derive the growth rate of the voids located in the matrix.
- Finally, in the last section, we discussed the results of our analylical solutions with and without the presence of the porosity.

2 Presentation of the Hollow Porous Sphere Problem

We consider a hollow sphere of inner radius a_0, outer radius b_0, representing an elementary cell of a porous plastic metal, see Figure 1.1. The matrix contains secondary small, dispersed voids; its porosity is initially uniform and denoted f_2^0. The boundary of the central void is free of traction whereas the outer boundary is subjected to some overall hydrostatic tension $\boldsymbol{\Sigma}_m$. The details of the derivation of these boundary conditions can be found in Appendix 7. The matrix material of the porous hollow sphere is supposed to obey the GLPD constitutive model as described in Appendix 6 and in [19]. The hollow sphere model problem presented here have served to find the solutions of several ductile fracture problems the solution of which have yields micromechanics based models for ductile porous metals under various loading conditions. Some of these problems as well as their solutions can be found in the works of [22], [23], and [8, 9] to mention a few of them.

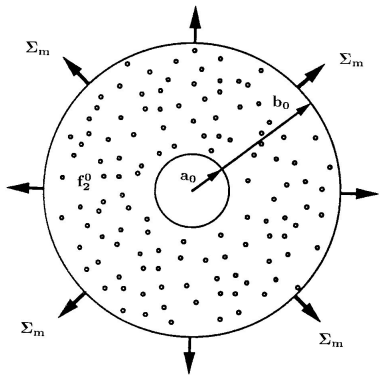

Fig. 1 The hollow sphere model problem considered

3 Analytical Solution When the Porosity is Neglected

3.1 Derivation of the Mechanical Fields

We are seeking a solution of the spherical shell problem for purely ideal-plastic behavior, the yield stress in simple tension being denoted by Σ_0 and the porosity in the matrix neglected. As a result, the yield criterion Eq.(48) reduces

$$\Phi(\boldsymbol{\Sigma}, \boldsymbol{M}, \Sigma) \equiv \frac{1}{\bar{\Sigma}^2}\left(\Sigma_{eq}^2 + \frac{Q^2}{b^2}\right) - 1 = 0. \tag{1}$$

. In this equation $\boldsymbol{\Sigma}$ represents the ordinary second-rank symmetric Cauchy stress tensor and $\boldsymbol{M}$ is the third-rank "moment tensor" symmetric in its first two indices only. The components of $\boldsymbol{M}$ are related through the conditions.

$$M_{ijj} = 0. \tag{2}$$

In the same expression:

- $\Sigma_{eq} \equiv \left(\frac{3}{2}\boldsymbol{\Sigma}' : \boldsymbol{\Sigma}'\right)^{1/2}$ ($\boldsymbol{\Sigma}'$: deviator of $\boldsymbol{\Sigma}$) is the von Mises equivalent stress.
- Σ represents a kind of average value of the yield stress in the heterogeneous metallic matrix.
- Q^2 is a quadratic form of the components of the moment tensor given by

$$Q^2 \equiv A_1\mathcal{M}_1 + A_2\mathcal{M}_2 \quad , \quad \begin{cases} A_1 = 0.194 \\ A_2 = 6.108 \end{cases} \tag{3}$$

  where $\mathcal{M}_1$ and $\mathcal{M}_2$ are the quadratic invariants of $\mathbf{M}$ defined by:

$$\begin{cases} \mathcal{M}_1 \equiv M_{mi}M_{mi} \\ \mathcal{M}_2 \equiv \frac{3}{2}M'_{ijk}M'_{ijk}, \end{cases} \tag{4}$$

  $M_{mi} \equiv \frac{1}{3}M_{hhi}$ and $\mathbf{M}'$ denoting the mean and deviatoric parts of $\mathbf{M}$, taken over its first two indices.
- b represents the characteristic lenght scale.

The flow rule, Eq.(52), becomes, after development (see [8, 18] for the details),

$$\begin{cases} \dot{D}^p_{ij} = \eta\dfrac{3}{\Sigma_0^2}\,\Sigma'_{ij} \\ \\ \left(\nabla\dot{D}\right)^p_{ijk} = \dfrac{\eta}{{\Sigma_0}^2 b^2}\left(\dfrac{2}{3}A_I\delta_{ij}M_{mk} + 3A_{II}M'_{ijk}\right) + \delta_{ik}U_j + \delta_{jk}U_i, \end{cases} \tag{5}$$

$M_{mk} \equiv \frac{1}{3}M_{hhk}$ and $\boldsymbol{M'}$ denoting the mean and deviatoric parts of $\boldsymbol{M}$, taken over its first two indices; η is the plastic multiplier, determined from the consistency condition and defined as

$$\eta = \left\{ \begin{array}{lll} = 0 & \text{if} & \Phi(\boldsymbol{\Sigma}, \mathbf{M}, \Sigma) < 0 \\ \geq 0 & \text{if} & \Phi(\boldsymbol{\Sigma}, \mathbf{M}, \Sigma) = 0. \end{array} \right\}$$

We shall also assume that the parameter A_I=0 for the analytical solution to be amenable. Another, more elaborate reason for this choice is that the value of A_I in the GLPD model, 0.194, is very small with respect to that of A_{II}, 6.108; hence, the value of A_I can safely be neglected. The remaining equations of the GLPD constitutive relations for ductile porous

materialas can be found in Appendix 6 and in [19].

We are looking for a solution in which the spherical shell is entirely plastic, so that the yield function $\Phi(\boldsymbol{\Sigma}, \boldsymbol{M}, \Sigma_0)$ is zero everywhere. Since such a solution was already presented in [10], only a summary of the procedure is given in this work. Let us consider the velocity, strain rate and its gradient fields first. As in the case of purely elastic behavior, the matrix of spherical shell is incompressible; as a result, the velocity field is radial and given by

$$\mathcal{U} = \frac{A}{r^2}, \tag{6}$$

where A is a parameter which is independent of the material point position r.

The non-zero components of the stress and moment fields are found using the flow rule and the incompressibility of the material. These components are obtained as

$$\begin{cases} \Sigma'_{rr} = \dfrac{1}{\eta}\left(-\dfrac{2A\Sigma_0^2}{3r^2}\right) \\ \Sigma'_{\theta\theta} = \Sigma'_{\phi\phi} = \dfrac{1}{\eta}\left(\dfrac{A\Sigma_0^2}{3r^2}\right) \end{cases} \tag{7}$$

and

$$\begin{cases} M'_{rrr} = \dfrac{1}{\eta}\dfrac{2A\Sigma_0^2 b^2}{A_{II} r^4} \\ M'_{\theta\theta r} = M'_{\phi\phi r} = -\dfrac{1}{\eta}\dfrac{A\Sigma_0^2 b^2}{A_{II} r^4} \\ M_{r\theta\theta} = M_{r\phi\phi} = -\dfrac{1}{\eta}\dfrac{A\Sigma_0^2 b^2}{A_{II} r^4} \end{cases} \tag{8}$$

The conditions $M_{ijj} = 0$ and a combination of the definitions of M'_{rrr} and $M_{r\theta\theta}$ given by the relations Eq.$(8)_1$ and Eq.$(8)_3$ yield

$$\begin{cases} M_{rrr} = -2M_{r\theta\theta} \\ M_{\theta\theta r} = M'_{\theta\theta r}. \end{cases} \tag{9}$$

Replacing the formulas for the stress Eq.(7) and moment Eq.(8) in the reduced yield criterion, Eq.(1), we get the following expression for the plastic multiplier η:

$$\eta = \frac{A\Sigma_0}{r^3}\sqrt{1 + \frac{15}{A_{II}}\frac{b^2}{r^2}}. \tag{10}$$

The explicit relation of the plastic multiplier Eq.(10) completes the definition of the non-zero components of the moment tensor. However, the full expressions of the non-zero components of the ordinary stress tensor are still unknown. After a tedious but straightforward calculation which uses (i) the expressions of the non-zero components of the moment tensor, (ii) the spherical symmetry properties of the problem, and (iii) the fact that $\Sigma_{rr} - \Sigma_{\theta\theta} = \Sigma'_{rr} - \Sigma'_{\theta\theta}$, the formulas for the non-zero components of the ordinary Cauchy stress tensor are obtained as

$$\frac{d\Sigma_{rr}}{dr} = f(r) \tag{11}$$

with

$$\begin{cases} f(r) = \dfrac{2A\Sigma_0^2}{\eta r^3} + \dfrac{2(\eta''\eta^2 - 2\eta'^2\eta)}{\eta^4}\dfrac{A\Sigma_0^2 b^2}{A_{II} r^4} - \dfrac{28\eta'}{\eta^2}\dfrac{A\Sigma_0^2 b^2}{A_{II} r^5} \\ -\left(\dfrac{72}{\eta} + \dfrac{2\eta'}{\eta^2}\right)\dfrac{A\Sigma_0^2 b^2}{A_{II} r^6} - \dfrac{8A\Sigma_0^2 b^2}{\eta A_{II} r^7} \end{cases} \tag{12}$$

where η' and η'' denote the first and second derivatives of the plastic multiplier η with respect to r. Eq.(11) implicitly defines the expression of the component Σ_{rr} of the stress tensor. The non-zero components of the stress tensor are obtained as

$$\Sigma_{rr} = \int_{r_i}^{r} f(\tau)d\tau; \quad \Sigma_{\theta\theta} = \Sigma_{\phi\phi} = \Sigma_{rr} - \frac{1}{\eta}\left(\frac{A\Sigma_0^2}{r^2}\right). \tag{13}$$

The solution of Eq.(13) along with the non-zero components of the moment provided above automatically satisfy the balance equations.

Quantity	Symbol	Unit	Value
internal radius	r_i	m	0.05
yield stress	Σ_0	MPa	100
parameter 1	A	m	0.001
parameter 2	A_1	-	0.194
parameter 3	A_2	-	6.108

Table 1 List of constants parameters

3.2 Numerical Illustrations of the Solution

The purpose of this section is to illustrate the analytical solution presented in [14]. More specifically, we derive the explicit expressions for the stress and moment tensors left off from [14]'s results. We do so by evaluating the integral Eq.(13) using a FORTRAN routine we developed. Each integral has also been evaluated analytically so that we possess the exact solution. Table 1 identifies the material and model parameters that are used to obtain the results mentioned in this work. Figures 3.1 (a), (b), and (c) illustrate the solutions for the stress components Σ_{rr}, $\Sigma_{\theta\theta}$, and the moment components M_{rrr} and $M_{r\theta\theta}$, respectfully. Figure 3.1 illustrate the analytical expressions of the non zero components of the Cauchy stress and the moment tensors as obtained in [10]. The figure shows that singularities are absent from the stress. Also, there is no discontinuity near the void as the Gurson model would have predicted.

4 Analytical Solution in the Presence of Porosity in the Matrix

In this section we present the solution to the hollow sphere problem for the case where the matrix obeys the full GLPD model. Therefore, we loose the simplification that yields the prior results [10]. A detailed derivation of the solution is presented in Burson and Enakoutsa [4]. Only some elements of such solution are presented in what follows.

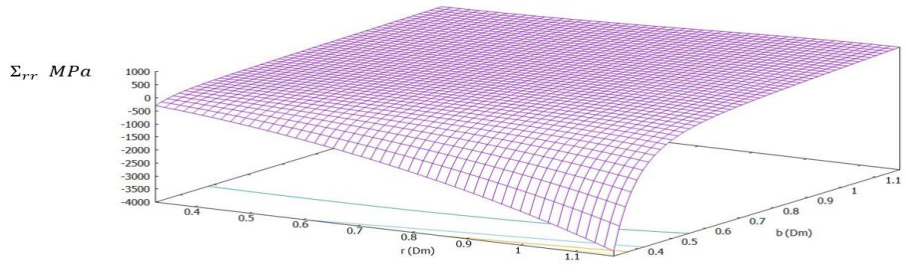

(a) Surface of the stress component Σ_{rr}

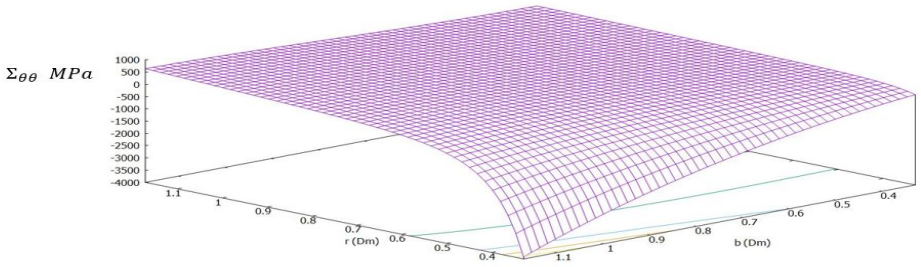

(b) Surface of the stress component $\Sigma_{\theta\theta}$

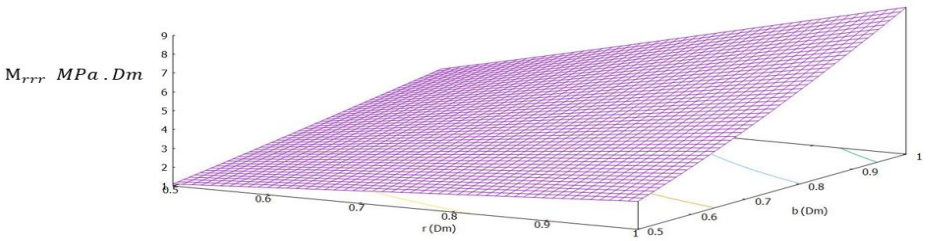

(c) Surface of the moment component M_{rrr}

Fig. 2 Illustration of the stress components Σ_{rr}, $\Sigma_{\theta\theta}$ and moment component M_{rrr}. These three mechanical fields are represented in the form of surfaces where the independent variables are the radius r and the characteristic length scale b. The surfaces obtained are all smooth; in particular, the singularity in the Cauchy stress obtained with first gradient model are been smoothed out with second gradient model effects.

4.1 Derivation of Cauchy Stress Components

The setup of the problem is provided by the balance equations of the problem which are provided in [10], the yield criterion, and the booundary conditions which are given in [10]:

$$\begin{cases} \dfrac{d\Sigma_{rr}}{dr} + \dfrac{2}{r}(\Sigma_{rr} - \Sigma_{\theta\theta}) - \dfrac{d^2 M_{rrr}}{dr^2} - \dfrac{4}{r}\dfrac{dM_{rrr}}{dr} - \dfrac{2}{r^2}M_{rrr} \\ \qquad + \dfrac{2}{r^2}\dfrac{dM_{\theta\theta r}}{dr} + \dfrac{4}{r}\dfrac{dM_{r\theta\theta}}{dr} + \dfrac{8}{r^2}M_{r\theta\theta} = 0 \qquad (14.a) \\ \dfrac{1}{\Sigma^2}\left(\Sigma_{eq}^2 + \dfrac{Q^2}{b^2}\right) + 2p\cosh\left(\dfrac{3}{2}\dfrac{\Sigma_m}{\Sigma}\right) - 1 - p^2 = 0, \qquad (14.b) \end{cases}$$

with M_{rrr} and $M_{r\theta\theta}$ the components of the moment tensor $\mathbf{M}$, Σ_{rr} and $\Sigma_{\theta\theta}$ the non zero components of the stress tensor $\mathbf{\Sigma}$, Σ_m the mean stress, Σ_{eq} the Von Mises stress. The boundary conditions are

$$\begin{cases} r^2\Sigma_{rr} - \dfrac{d\left(r^2 M_{rrr}\right)}{dr} + 4rM_{r\theta\theta} = 0, \\ M_{rrr} = 0 \end{cases}$$

for $r = r_i$ and $r = r_e$.

The stress components Σ_{rr} and $\Sigma_{\theta\theta}$ in the balance equation Eq.(14.a) can be expressed in terms of the invariants Σ_m and Σ_{eq} as followed

$$\frac{d\Sigma_{rr}}{dr} + \frac{2}{r}(\Sigma_{rr} - \Sigma_{\theta\theta}) = \frac{2}{3\sqrt{3}}\frac{d}{dr}\Sigma_{eq} + \frac{2}{r\sqrt{3}}\Sigma_{eq} + \frac{d}{dr}\Sigma_m \tag{15}$$

The formulation for Σ_{eq} is determined by the differential equation

$$\frac{d}{dr}\Sigma_{eq} = \frac{\alpha(\Sigma_0 - \Sigma_{eq}^2) - \dfrac{6}{r}\Sigma_{eq}\left(\sqrt{\Sigma_0 - \Sigma_{eq}^2}\right) + \lambda}{\sqrt{\Sigma_0 - \Sigma_{eq}^2} - \beta\Sigma_{eq}} \tag{16}$$

From here we completely solve for Σ_{eq} and Σ_m for which we easily deduce Σ_{rr} and Σ_θ by solving the linear system

$$\begin{pmatrix} \Sigma_{eq} \\ \Sigma_m \end{pmatrix} = \begin{pmatrix} \sqrt{3} & -\sqrt{3} \\ 1 & 2 \end{pmatrix} \begin{pmatrix} \Sigma_{rr} \\ \Sigma_{\theta\theta} \end{pmatrix} \tag{17}$$

The solution is

$$\begin{pmatrix} \Sigma_{rr} \\ \Sigma_{\theta\theta} \end{pmatrix} = \frac{1}{3\sqrt{3}} \begin{pmatrix} 2 & \sqrt{3} \\ -1 & \sqrt{3} \end{pmatrix} \begin{pmatrix} \Sigma_{eq} \\ \Sigma_m \end{pmatrix} \tag{18}$$

or simply

$$\begin{pmatrix} \Sigma_{rr} = \dfrac{2}{3\sqrt{3}}\Sigma_{eq} + \dfrac{1}{3}\Sigma_m, \\ \Sigma_{\theta\theta} = \dfrac{1}{3}\Sigma_m - \dfrac{1}{3\sqrt{3}}\Sigma_{eq} \end{pmatrix}$$

4.2 Derivation of the Moment Tensor Components

In this section we derive the components of the moment tensor $\mathbf{M}$. The moment components M_{ijk} are recovered by the use of the flow rule and the velocity field, which we assume can be represented as

$$\mathcal{U} = (f(r), 0, 0)$$

for some function $f(r)$ depending on the spherical radial coordinate r. With this assumption the GLPD flow rule reduces to

$$\nabla D_{mk} = \frac{2}{3}\eta U_k$$

where η is the plastic multiplier and U the velocity field (see [10] for exact details.) In accordance with Eq.(36) in [10] when $A_1 = 0$ the strain rate components are

$$\begin{cases} (\nabla D)_{rrr} &= \dfrac{df}{dr} = \dfrac{\eta}{\Sigma_0^2 b^2} 3A_2 M'_{rrr} \\ (\nabla D)_{r\theta\theta} &= 0 = \dfrac{\eta}{\Sigma_0^2 b^2} 3A_2 M'_{\theta\theta r} \\ (\nabla D)_{\theta\theta r} &= \dfrac{1}{r}\dfrac{df}{dr} = \dfrac{\eta}{\Sigma_0^2 b^2} 3A_2 M'_{r\theta\theta} \\ (\nabla D)_{r\phi\phi} &= \dfrac{1}{r}\dfrac{df}{dr} = \dfrac{\eta}{\Sigma_0^2 b^2} 3A_2 M_{r\theta\theta} \end{cases} \tag{20}$$

Let $\kappa = \dfrac{\Sigma_0^2 b^2}{3A_2}$ then the deviatoric parts of the moment $\mathbf{M}$ satisfy

$$M'_{rrr} = \frac{\kappa}{\eta}\frac{df}{dr}, \quad M'_{\theta\theta r} = 0, \quad M'_{r\theta\theta} = \frac{\kappa}{\eta}\frac{1}{r}\frac{df}{dr}, \quad M_{r\theta\theta} = \frac{\kappa}{\eta}\frac{1}{r}\frac{df}{dr}.$$

The value of Q^2 then is computed as follows

$$Q^2 = \frac{3}{2}A_2\left(\frac{df}{dr}\frac{\kappa}{\eta}\right)^2\left(\frac{r^2+1}{r^2}\right) \tag{21}$$

Using the yield criterion we found that the function f satisfies the ordinary differential equation

$$\left(\frac{df}{dr}\right)^2 = \frac{2}{3A_2}\left(\frac{\eta}{\kappa}\right)^2\left(\frac{r^2}{r^2+1}\right)b^2\left(\Sigma^2\left(p^2+1-2p\cosh\left(\frac{3}{2}\frac{\Sigma_m}{\Sigma}\right)\right)-\Sigma_{eq}^2\right)$$

Using Eq.(37) in [10] we get the devatoric part of the stress

$$\Sigma'_{rr} = -\frac{\Sigma_0^2}{3}\frac{1}{\eta}f(r), \quad \Sigma'_{\theta\theta} = \frac{\Sigma_0^2}{3}\frac{1}{\eta}f(r). \tag{22}$$

and from there the plastic multiplier satisifies

$$\eta = \frac{\Sigma_0^2}{2}\frac{f(r)}{\left(\Sigma_m - \dfrac{1}{\sqrt{3}\Sigma_{eq}}\right)} \tag{23}$$

where Σ_m and Σ_{eq} are provided in the previous section. Substituting Eq.(23) into Eq.(22) yields

$$\left(\frac{df}{dr}\right)^2 = f(r)^2 p(r) \tag{24}$$

where $p(r)$

$$p(r) = h(r)\iota(r)j(r)$$

with

$$\iota(r) = \left(\frac{\Sigma_0^4}{6(\Sigma_m - \frac{1}{\sqrt{3}\Sigma_{eq}})^2\kappa^2 A_2}\right), \quad j(r) = \left(\frac{r^2}{r^2+1}\right),$$

and

$$h(r) = \left(b^2\left(\Sigma^2\left(p^2 + 1 - 2p\,\cosh\left(\frac{3}{2}\frac{\Sigma_m}{\Sigma}\right)\right) - \Sigma_{eq}^2\right).$$

Next, the non zero components of the moment are recovered by the formulas Eq.(20)

$$\begin{cases} M'_{rrr} = \frac{\kappa}{\eta}\frac{df}{dr} \\ M'_{\theta\theta r} = M'_{\phi\phi r} = \frac{-\kappa}{\eta}\frac{1}{r}\frac{df}{dr} \\ M'_{r\theta\theta} = M_{r\theta\theta} = \frac{\kappa}{\eta}\frac{1}{r}\frac{df}{dr} \end{cases} \tag{26}$$

where η and κ are again given as

$$\begin{cases} \eta = \frac{\Sigma_0^2}{2}\frac{f(r)}{\left(\Sigma_m - \frac{1}{\sqrt{3}\Sigma_{eq}}\right)} \\ \kappa = \frac{\Sigma_0^2 b^2}{3A_2} \end{cases}$$

The conditions $M_{ijj} = 0$ relate the rest of the non-zero components of the moment tensor, M_{rrr} and $M_{r\theta\theta}$ as follows:

$$M_{rrr} + 2M_{r\theta\theta} = 0 \tag{28}$$

Furthermore, we find

$$M_{mr} = M_{rrr} - M'_{rrr} = 2M_{r\theta\theta} - M'_{rrr} \tag{29}$$

where M_{mr} denotes the deviatoric part of the tensor $\mathbf{M}$ over its first two indices. The formula immediately yields $M_{\theta\theta r} = M'_{\theta\theta r}$. The formula Eq.(29) immediatly gives

$$M_{r\theta\theta} = M'_{\theta\theta r} \tag{30}$$

Figures 3.1 (A) and (B)) illustrates the radial distribution of the equivalent (Case **A**) and mean stresses (Case **B**), respectively, obtained from the analytical solution we developped in this paper. On a radius of the hollow sphere matrix material, Σ_{eq} increases from the inner surface to the external one while the situation in the reverse order occurs for Σ_m. The latter behavior seems to confirm strong triaxaility effects in the vicinity of the inner surface of the hollow sphere structure which is usually due to loading histories. There is a need to develop a full solution of the model problem (involving porosity effects) to confirm this trend.

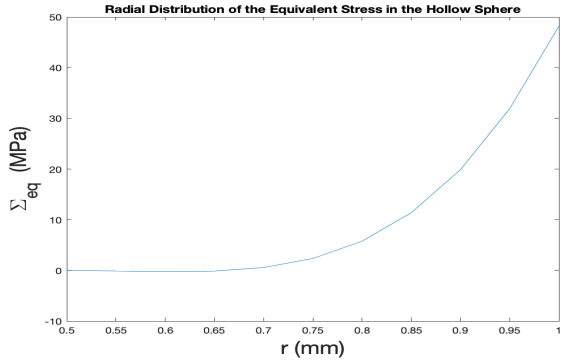

(A) Distribution of Σ_{eq} in the matrix material.

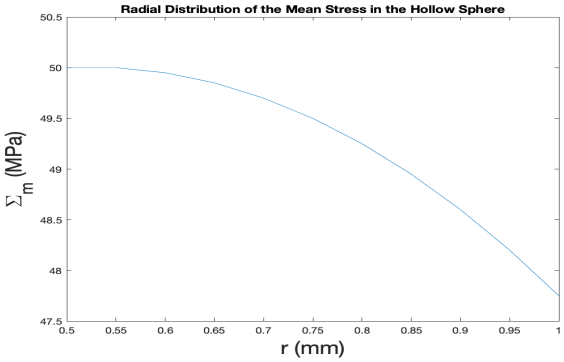

(B) Distribution of Σ_m in the matrix material.

Fig. 3 Illustration of the radial equivalent and mean stresses, Σ_{eq} in (**A**), Σ_m in (**B**) of the Cauchy stress tensor

4.3 Derivation of the Velocity Field

This section presents the analytical solution to the velocity field of the problem model presented. Following the same procedure in [22] we use the results obtained for the stress invariants to rewrite the flow rule in order to obtain a new differential equation involving the velocity. Recall that $d_m = \frac{1}{3}\mathrm{tr}(\mathbf{D}')$ and $d_{eq} = \frac{2}{3}(\mathbf{D}' : \mathbf{D}')^{2/3}$ where $\mathbf{D}'$ is the deviator of $\mathbf{D} = \frac{1}{2}\left[\nabla \mathcal{U} + (\nabla \mathcal{U})^t\right]$. Following Leblond's calculation [22, p. 97] we find

$$\frac{d_m}{d_{eq}} = \frac{\mathrm{tr}(\mathbf{D}')}{2(\mathbf{D}' : \mathbf{D}')^{1/2}} = \frac{\dfrac{d\mathcal{U}}{dr} + \dfrac{2\mathcal{U}}{r}}{2\left(\dfrac{\mathcal{U}}{r} - \dfrac{d\mathcal{U}}{r}\right)} = \frac{p}{2}\frac{\Sigma_0}{\Sigma_{eq}}\sinh\left(\frac{3}{2}\frac{\Sigma_m}{\Sigma_0}\right). \tag{31}$$

Here the right hand side is derived from the elimination of the plastic multiplier between the deviatoric and mean parts of the homogenized flow rule. Using the yield criterion we may rewrite the right hand side

$$\frac{p}{2}\frac{\Sigma_0}{\Sigma_{eq}}\sinh\left(\frac{3}{2}\frac{\Sigma_m}{\Sigma_0}\right)=\frac{p}{2}\frac{\Sigma_0}{\Sigma_{eq}}\sqrt{\frac{\Sigma_0^4}{4p^2}\left(p^2+1-\left(\frac{\Sigma_{eq}^2}{\Sigma_0^2}+\frac{Q^2}{b^2\Sigma_0^2}\right)\right)-1} \tag{32}$$

so that the velocity warrants itself as a function of both the stress and moments. Consider φ defined explicitly as

$$\varphi(r)=\frac{p}{2}\frac{\Sigma_0}{\Sigma_{eq}}\sqrt{\frac{\Sigma_0^4}{4p^2}\left(p^2+1-\left(\frac{\Sigma_{eq}^2}{\Sigma_0^2}+\frac{Q^2}{b^2\Sigma_0^2}\right)\right)-1}.$$

Then the ordinary differtnial equation for the velocity is

$$\frac{\dfrac{d\mathcal{U}}{dr}+\dfrac{2\mathcal{U}}{r}}{2\left(\dfrac{\mathcal{U}}{r}-\dfrac{d\mathcal{U}}{r}\right)}=\varphi(r). \tag{33}$$

The above may be rewritten as

$$\frac{d\mathcal{U}}{dr}+g(r)\mathcal{U}=0,\quad \text{with}\quad g(r):=\frac{2}{r}\frac{(1-\varphi(r))}{(1+2\varphi(r))} \tag{34}$$

which is a first ordinary linear differntial equation. The general solution to Eq.(34) is well known and provided by the formula

$$\mathcal{U}(r)=\lambda\exp\left[-\int_{r_0}^{r}g(\tau)d\tau\right] \tag{35}$$

where λ is a constant velocity determined from the velocity at some point in the matrix.

4.4 The Growth Rate of the Voids

The full solution for the stress, moments and velocity field allows us to completely determine the growth rate of voids in the matrix. From the evolution of internal parameters the growth of voids satisfy

$$-\frac{d}{dt}\ln(1-f)=d_m. \tag{36}$$

Taking into account the general solution to the velocity field

$$d_m=\frac{d\mathcal{U}}{dr}+\frac{2\mathcal{U}}{r}=\lambda\exp\left[-\int_{r_0}^{r}p(\tau)d\tau\right]\left(p(r)+\frac{2}{r}\right),$$

the growth of voids is given as

$$f=1-\exp\left[\int_{r_0}^{r}\xi(\gamma)d\gamma\right] \tag{37}$$

with ξ provided by the formula

$$\xi(\gamma)=\lambda\exp\left[-\int_{r_0}^{\gamma}g(\tau)d\tau\right]\left(g(\gamma)+\frac{2}{\gamma}\right).$$

The porous material's matrix contains small voids and a matrix that is incompressible; the dilatation $div(\mathcal{U}(r)e_r)$ is associated to a growth $\dot{f}_2(r)$ of the porosity at the points located at a distance r of the central void, or equivalently to a gowth of the mean radius, ρ, of the small cavities located at this position. Standard derivations based on incompressibility of the sound (void-free) matrix have demonstrated that the growth rate $\frac{\dot{\rho}}{\rho}$ of secondary voids is given by

$$\frac{\dot{\rho}}{\rho} = \frac{\dot{f}_2}{3f_2^0\,(1-f_2^0)} = \frac{div(\mathcal{U}(r)e_r)}{f_2^0} = \frac{d_m}{f_2^0}. \tag{38}$$

For small values of the of the porosity f_2^0 (which is the case for practical reasons, Eq.(38) becomes

$$\frac{\dot{\rho}}{\rho} = \frac{\dot{f}_2}{3f_2^0} = \frac{\dot{a}}{f_2^0}\exp\left[-\int_{r_0}^{r} g(\tau)d\tau\right]\left(g(r)+\frac{2}{r}\right). \tag{39}$$

In the vicinity of the large void where $r = a_0$, Eq.(39) reduces

$$\frac{\dot{\rho}}{\rho}\,(r=a_0) = \frac{\dot{a}}{a_0}\left(f_2^0 p(a_0) + \frac{2}{f_2^0}\right). \tag{40}$$

Eq.(40) shows that the small voids located near the boundary of the big one grow logarithmically faster (the coefficient $f_2^0 p(a_0) + \frac{2}{f_2^0} \approx \frac{2}{f_2^0}$ as f_2^0 is very small) than the larger void.

4.5 Discussion

In this section we elaborate on some of the results found in this work. First, we observe that when the characteristic length scale vanishes then all of the components of the moment tensor also vanish by Eq.(20). This means that any second gradient effects in the GLPD model no longer exist. The yield criterion reduces to the original Gurson model yield criterion and the stress state of the material does not contain any length scale effects.

Next, unlike in the work of [10] where a vanishing porosity was considered, this work introduces a non vanishing porosity (at the initial time where the porosity has not yet evolved;) this will be sufficient to model ductile fracture mechanisms in metals with two populations of cavities. The study of porosity effects after the initial time is left for future investigations. However, let us mention that the works of Perrin and Leblond [22, 23] have addressed these features, but the model their analysis is based on does not contain second gradient effects.

Furthermore, the boundary conditions $M_{rrr}(r = r_i, r_e) = 0$ ensures that the model does not account for boundary layer effects. Also, these boundary conditions induce no shear component effects.

Finally, the expression of the void growth rate of the small voids in the matrix of the hollow sphere suggests that small voids located at the boundary of the large central void grow much more rapidly than the latter; this effect was first pointed out by Perrin and Leblond [22, 23] in the absence of nucleation, and is further enhanced by nucleation as demonstrated by [14, 17]. As a consequence, the small voids may reach coalescence before the large central

one. The presence of length scale effects in the growth rate will add microstructure effects on the fracture mechanisms pointed out above.

5 Conclusion

In this work we develop a solution for the micromorphic hollow sphere model under tension obeying the GLPD constitutive model when the porosity is constant at the initial time and we illustrate the analytic solutions provided previously by Enakousta's work when the porosity is neglected, but some effects of the strain gradient were involved. We express the stress solutions in terms of the invariants of the Cauchy stress tensor. The solution of the nonzero components of the moments due to the strain gradient effects are also provided in this work.The radial velocity field and the growth rate of the small voids located in the matrix are derived; the expression of the latter suggest that small voids located near the larger one grow faster to form a shell of ruined material around the large void, a scenario that agrees very well with experimental observations. In addition, the solution developed in this work depends on the characteristic length scale and can be used as benchmark solution to assess micromorphic gradient models; the solution can also be used to test the efficiency of numerical implementation of gradient models into finite element software.

References

1. Ahad, F., Enakoutsa, K., Solanki, K., and Bammann, D. 2013. Nonlocal Modeling in High Velocity Impact failure of Aluminum 6160-T6, *Int. J. Plast.,* **55**, 108-132
2. Andreaus, U., dell'Isola, F., Giorgio, I., Placidi, L., Lekszycki, T., Rizzi, N. L. 2016. Numerical simulations of classical problems in two-dimensional (non) linear second gradient elasticity. International Journal of Engineering Science, 108, 34-50.
3. Bergheau, J-M, Leblond, J-B, Perrin, G. 2013. A New Numerical Implementation of a second-gradient model for plastic porous solids, with an application of ductile rupture tests, *Computer Methods in Applied Mechanics and Engineering,* **268**, 105-125
4. Burson, R., Enakoutsa, K. (2022). Closed-form Analytic Solutions of the Problem of a Hollow Sphere Made of Second Gradient Plastic Porous Material and Subjected to Hydrostatic Loading. In: Giorgio, I., Placidi, L., Barchiesi, E., Abali, B.E., Altenbach, H. (eds) Theoretical Analyses, Computations, and Experiments of Multiscale Materials. Advanced Structured Materials, vol **175**. Springer, Cham. https://doi.org/10.1007/978-3-031-04548-6
5. dell'Isola, F., Della Corte, A., Giorgio, I. 2017. Higher-gradient continua: The legacy of Piola, Mindlin, Sedov and Toupin and some future research perspectives. *Mathematics and Mechanics of Solids*, **22**(4), 852-872.
6. Gurson, Arthur L. 1977. Continuum theory of ductile rupture by void nucleation and growth: Part I Yield criteria and flow rules for porous ductile media.*J of Eng. Mater. Technol*, **99**(1), 2-15.
7. Giorgio, I., Andreaus, U., dell'Isola, F., Lekszycki, T. 2017. Viscous second gradient porous materials for bones reconstructed with bio-resorbable grafts. *Extreme Mechanics Letters*, **13**, 141-147.
8. Enakoutsa, K., 2007. Modèle Non-locaux en Rupture Ductile des Métaux. Ph.D thesis, Université Pierre et Marie Curie (Paris VI) (in French)
9. Enakoutsa, K., 2012. Some new Applications of the GLPD Micromorphic Model of Ductile Fracture. *Mathematics and Mechanics of Solids,* **19**(3), 242-259
10. Enakoutsa, K. 2013. Exact results for the problem of a hollow sphere subjected to hydrostatic tension and made of micromorphic plastic porous material. *Mechanics Research Communications* **49**, 1-7.
11. Enakoutsa K., Leblond J.B. and Perrin G. 2007. Numerical implementation and assessment of a phenomenological nonlocal model of ductile rupture, *Comput. Meth. Appl. Mech. Engng.*, **196**, 1946-1957
12. Enakoutsa, K., Solanki, K., Ahad, F., Tjiptowidjojo, Y., and Bammann, D. 2012. Using Damage Delocalization to Model Localization Phenomena in Bammann-Chiesa-Johnson Metals, *J. Eng. Mater. Tech.,* **134**(4)

13. Enakoutsa, K., Solanki, K., Ahad, F., Tjiptowidjojo, Y., and Bammann, D. 2012. Damage smoothing effects in a delocalized rate sensitivity model for metals, *Theoretical and Applied Mechanical Letters,* **2**(5): 5-051005
14. Enakoutsa, K. 2013. Exact results for the problem of a hollow sphere subjected to hydrostatic tension and made of micromorphic plastic porous materials, *Mech. Res. Commun.,* **49**, 1-7
15. Enakoutsa, K. 2013. An Analytic Benchmark Solution to the Problem of a Generalized Plane Strain Hollow Cylinder made of Micromorphic Plastic Porous Metal and Subjected Axisymmetric Loading Conditions, *Math. Mech. Solids,* **9**, 1013-1025
16. Enakoutsa, K. 2013. Modeling ductile fracture in metals involving two populations of voids influence of continuous nucleation of secondary voids upon growth and coalescence of primary voids, , *Math. Mech. Solids,* **18**3, 323-345
17. Enakoutsa K, Leblond J-B, Audoly B. Influence of continuous nucleation of secondary voids upon growth and coalescence of cavities in porous ductile metals. In: Carpinteri A, editor. Proceedings of the 11th international conference on fracture, March 2025, Turin, Italy, CD-Rom, 2005.
18. Enakoutsa K., and Leblond J.B., 2009. Numerical Implementation and Assessment of the GLPD Micromorphic Model of Ductile Rupture. *European Journal of Mechanics A/Solids*, **28**, 445-460
19. Gologanu M., Leblond J.B., Perrin G. and Devaux J. 1997. Recent extensions of Gurson's model for porous ductile metals, in: *Continuum Micromechanics*, CISM Courses and Lectures 377, P. Suquet ed., Springer, pp. 61-130
20. Gurson A.L. 1977. Continuum theory of ductile rupture by void nucleation and growth: Part I - yield criteria and flow rules for porous ductile media, *ASME J. Engng. Mater. Technol.*, **99**, 2-15
21. Leblond, J.B., Perrin, G., and Devaux, J. 1994. Bifurcation Effects in Ductile Metals with Nonlocal Damage, *ASME J. Applied . Mech.*, **6**1, 236-242.
22. Perrin, G, and Leblond, JB 2000. Accelerated void growth in porous ductile solids containing two populations of cavities. *Int. J. Plast.,* **16**, 91v120
23. Perrin, G, and Leblond, J-B, 1990. Analytical study of a hollow sphere made of plastic porous material and subjected to hydrostatic tension Application to some problems in ductile fracture of metals, *Int. J. Plast.,* **6**:677699
24. Pijaudier-Cabot, G. and Bazant, Z.P., 1987. Nonlocal Damage Theory, *ASCE J. Engrg. Mech.*, **1**13, 1512-1533
25. Placidi, L., Barchiesi, E., Misra, A., Timofeev, D. 2021. Micromechanics-based elasto-plasticity damage energy formulation for strain gradient solids with granular microstructure. Continuum Mechanics and Thermodynamics, **33**, 2213-2241
26. Nahshon, K., Hutchinson, J.W., 2008. Modification of the Gurson model for shear failure, *Eur. J. Mech. A/Solids,* **27**, 1-17.
27. Rice, J. R. and Tracey, D. M. 1969. On the Ductile Enlargement of Voids in Triaxial Growth Holes. *J. Mech. Phys. Solids,* **17**, 210-217
28. Tvergaard V. and Needleman A. 1997. Nonlocal effects on localization in a void-sheet, *Int. J. Solids Structures,* **34**, 2221-2238
29. Tvergaard V. and Needleman A. 1995. Effects of nonlocal damage in porous plastic solids, *Int. J. Solids Structures,* **32**, 1063-1077 s
30. Reiher, J. C., Giorgio, I., Bertram, A. 2017. Finite-element analysis of polyhedra under point and line forces in second-strain gradient elasticity. Journal of Engineering Mechanics, **143**(2), 04016112.
31. Scerrato, D., Bersani, A. M., Giorgio, I. 2021. Bio-Inspired Design of a Porous Resorbable Scaffold for Bone Reconstruction: A Preliminary Study. *Biomimetics*, **6**(1), 18.
32. Tvergaard V. 1981. Influence of voids on shear band instabilities under plane strain conditions, *Int. J. Fracture*, **17**, 389-407.
33. Tvergaard V. and Needleman A. 1984. Analysis of cup-cone fracture in a round tensile bar, *Acta Metall.*,**32**, 157-169.

6 Appendix (a): The Constitutive Relations of the GLPD Model

6.1 Generalities

In the GLPD model, internal forces are represented through some ordinary second-rank symmetric Cauchy stress tensor $\boldsymbol{\Sigma}$ plus some additional third-rank "moment tensor" $\mathbf{M}$ symmetric in its first two indices only[2]. The components of $\mathbf{M}$ are related through the three conditions

$$M_{ijj} = 0. \tag{41}$$

(These conditions may be compared to the condition of plane stress in the theory of thin plates or shells). The virtual power of internal forces is given by the expression

$$\mathcal{P}^{(i)} \equiv -\int_{\Omega} (\boldsymbol{\Sigma} : \mathbf{D} + \mathbf{M} \vdots \nabla\mathbf{D})\, d\Omega \tag{42}$$

where Ω denotes the domain considered, $\mathbf{D} \equiv \frac{1}{2}\left[\nabla\mathbf{V} + (\nabla\mathbf{V})^T\right]$ ($\mathbf{V}$: material velocity) the Eulerian strain rate, $\nabla\mathbf{D}$ its gradient, $\boldsymbol{\Sigma} : \mathbf{D}$ the double inner product $\Sigma_{ij}D_{ij}$ and $\mathbf{M} \vdots \nabla\mathbf{D}$ the triple inner product $M_{ijk}D_{ij,k}$. The virtual power of external forces is given by

$$\mathcal{P}^{(e)} \equiv \int_{d\Omega} \mathbf{T}.\mathbf{V}\, dS \tag{43}$$

where $\mathbf{T}$ represents some surface traction[3].

The hypothesis of additivity of elastic and plastic strain rates reads

$$\begin{cases} \mathbf{D} & \equiv \mathbf{D}^e + \mathbf{D}^p \\ \nabla\mathbf{D} & \equiv (\nabla\mathbf{D})^e + (\nabla\mathbf{D})^p. \end{cases} \tag{44}$$

The elastic and plastic parts $(\nabla\mathbf{D})^e$, $(\nabla\mathbf{D})^p$ of the gradient of the strain rate here do *not* coincide in general with the gradients $\nabla(\mathbf{D}^e)$, $\nabla(\mathbf{D}^p)$ of the elastic and plastic parts of the strain rate.

6.2 Hypoelasticity law

The elastic parts of the strain rate and its gradient are related to the rates of the stress and moment tensors through the following hypoelasticity law:

$$\begin{cases} \dfrac{d\Sigma_{ij}}{dt} & = \lambda\,\delta_{ij}D^e_{kk} + 2\mu D^e_{ij} \\ \dfrac{dM_{ijk}}{dt} & = \dfrac{b^2}{5}\Big[\lambda\,\delta_{ij}(\nabla D)^e_{hhk} + 2\mu(\nabla D)^e_{ijk} \\ & \qquad -2\lambda\,\delta_{ij}U^e_k - 2\mu\left(\delta_{ik}U^e_j + \delta_{jk}U^e_i\right)\Big]. \end{cases} \tag{45}$$

[2] The component M_{ijk} is noted $M_{k|ij}$ in [19]'s original paper. The present notation leads to more natural-looking expressions.

[3] The general equilibrium equations and boundary conditions corresponding to the expressions (42) and (43) of the virtual powers of internal and external forces need not be given since they are not necessary for the numerical implementation.

In these expressions λ and μ denote the Lamé coefficients and b the mean half-spacing between neighboring voids. (In the homogenization procedure, b is the radius of the spherical elementary cell considered). Also, $\frac{d\Sigma_{ij}}{dt}$ and $\frac{dM_{ijk}}{dt}$ are the Jaumann (objective) time-derivatives of Σ_{ij} and M_{ijk}, given by

$$\begin{cases} \dfrac{d\Sigma_{ij}}{dt} & \equiv \dot{\Sigma}_{ij} + \Omega_{ki}\Sigma_{kj} + \Omega_{kj}\Sigma_{ik} \\ \dfrac{dM_{ijk}}{dt} & \equiv \dot{M}_{ijk} + \Omega_{hi}M_{hjk} + \Omega_{hj}M_{ihk} + \Omega_{hk}M_{ijh} \end{cases} \tag{46}$$

where $\boldsymbol{\Omega} \equiv \frac{1}{2}\left[\nabla\mathbf{V} - (\nabla\mathbf{V})^T\right]$ is the antisymmetric part of the velocity gradient. Finally $\mathbf{U}^e$ is a vector the value of which is fixed by equations (41) (written in rate form, $\frac{DM_{ijj}}{Dt} = 0$):

$$U_i^e = \frac{\lambda(\nabla D)^e_{hhi} + 2\mu(\nabla D)^e_{ihh}}{2\lambda + 8\mu}. \tag{47}$$

(This vector may be compared to the through-the-thickness component of the elastic strain rate in the theory of thin plates or shells, the value of which is fixed by the condition of plane stress).

6.3 Yield criterion

The plastic behavior is governed by the following Gurson-like criterion:

$$\frac{1}{\Sigma^2}\left(\Sigma_{eq}^2 + \frac{Q^2}{b^2}\right) + 2p\,\cosh\left(\frac{3}{2}\frac{\Sigma_m}{\Sigma}\right) - 1 - p^2 \leq 0. \tag{48}$$

In this expression:

- $\Sigma_{eq} \equiv \left(\frac{3}{2}\boldsymbol{\Sigma}' : \boldsymbol{\Sigma}'\right)^{1/2}$ ($\boldsymbol{\Sigma}'$: deviator of $\boldsymbol{\Sigma}$) is the von Mises equivalent stress.
- $\Sigma_m \equiv \frac{1}{3}\,\mathrm{tr}\,\boldsymbol{\Sigma}$ is the mean stress.
- Σ represents a kind of average value of the yield stress in the heterogeneous metallic matrix, the evolution equation of which is given below.
- p is a parameter connected to the porosity (void volume fraction) f through the relation:

$$p \equiv qf^*, f^* \equiv \begin{cases} f & \text{if } f \leq f_c \\ f_c + \delta(f - f_c) & \text{if } f > f_c \end{cases} \tag{49}$$

  where q is *Tvergaard's parameter*, f_c the *critical porosity at the onset of coalescence of voids*, and δ (> 1) a factor describing the accelerated degradation of the material during coalescence [32],[33].
- Q^2 is a quadratic form of the components of the moment tensor given by

$$Q^2 \equiv A_1\mathcal{M}_1 + A_2\mathcal{M}_2 \quad , \quad \begin{cases} A_1 = 0.194 \\ A_2 = 6.108 \end{cases} \tag{50}$$

  where $\mathcal{M}_1$ and $\mathcal{M}_2$ are the quadratic invariants of $\mathbf{M}$ defined by:

$$\begin{cases} \mathcal{M}_1 \equiv M_{mi}M_{mi} \\ \mathcal{M}_2 \equiv \frac{3}{2}M'_{ijk}M'_{ijk}, \end{cases} \tag{51}$$

$M_{mi} \equiv \frac{1}{3} M_{hhi}$ and $\mathbf{M}'$ denoting the mean and deviatoric parts of $\mathbf{M}$, taken over its first two indices.

- Again, b is the mean half-spacing between neighboring voids.

6.4 Flow rule

The plastic parts of the strain rate and its gradient are given by the flow rule associated to the criterion (48) through normality:

$$\left\{ \begin{array}{ll} D^p_{ij} & = \eta \dfrac{d\Phi}{d\Sigma_{ij}}(\boldsymbol{\Sigma}, \mathbf{M}, \Sigma, f) \\ (\nabla D)^p_{ijk} & = \eta \dfrac{d\Phi}{dM_{ijk}}(\boldsymbol{\Sigma}, \mathbf{M}, \Sigma, f) + \delta_{ik} U^p_j \\ & \quad + \delta_{jk} U^p_i \end{array} \right\} \tag{52}$$

where

$$\eta = \left\{ \begin{array}{lll} = 0 & \text{if} & \Phi(\boldsymbol{\Sigma}, \mathbf{M}, \Sigma, f) < 0 \\ \geq 0 & \text{if} & \Phi(\boldsymbol{\Sigma}, \mathbf{M}, \Sigma, f) = 0 \end{array} \right\}$$

The term $\delta_{ik} U^p_j + \delta_{jk} U^p_i$ in equation (52) represents a rigid-body motion of the elementary cell, which is left unspecified by the flow rule but fixed in practice by conditions (41). (The vector $\mathbf{U}^p$ may be compared to the through-the-thickness component of the plastic strain rate in the theory of thin plates or shells, the value of which is fixed by the condition of plane stress).

The values of the derivatives of the yield function $\Phi(\boldsymbol{\Sigma}, \mathbf{M}, \Sigma, f)$ in equations (52) are easily calculated to be

$$\left\{ \begin{array}{ll} \dfrac{d\Phi}{d\Sigma_{ij}}(\boldsymbol{\Sigma}, \mathbf{M}, \Sigma, f) & = 3 \dfrac{\Sigma'_{ij}}{\Sigma^2} + \dfrac{p}{\Sigma} \delta_{ij} \sinh\left(\dfrac{3}{2} \dfrac{\Sigma_m}{\Sigma} \right) \\ \dfrac{d\Phi}{dM_{ijk}}(\boldsymbol{\Sigma}, \mathbf{M}, \Sigma, f) & = \dfrac{1}{\Sigma^2 b^2} \left(\dfrac{2}{3} A_1 \delta_{ij} M_{mk} + 3 A_2 M'_{ijk} \right) \end{array} \right\} \tag{53}$$

6.5 Evolution of Internal Parameters

The evolution of the porosity is governed by the classical equation resulting from approximate incompressibility of the metallic matrix:

$$\dot{f} = (1 - f) \operatorname{tr} \mathbf{D}^p. \tag{54}$$

The parameter Σ is given by

$$\Sigma \equiv \Sigma(E) \tag{55}$$

where $\Sigma(\epsilon)$ is the function which provides the yield stress of the matrix material in terms of the local equivalent cumulated plastic strain ϵ, and E represents some average value of this equivalent strain in the heterogeneous matrix. The evolution of E is governed by the following equation:

$$(1 - f) \Sigma \dot{E} = \boldsymbol{\Sigma} : \mathbf{D}^p + \mathbf{M} \vdots (\nabla \mathbf{D})^p. \tag{56}$$

7 Appendix (b): Balance Equations and Boundary Conditions

The objective of this appendix is to present the details of the derivation of the equilibrium equations and boundary conditions, presented in Section 2. To do so, we shall apply the principle of virtual work with a radial velocity $\mathbf{v}^\star \equiv \mathrm{v}_\mathrm{r}^\star \mathrm{e}_\mathrm{r}$, instead of departing from the global equilibrium equations and calculating $\nabla\nabla\mathbf{M}$ in spherical coordinates. The virtual power of internal forces is defined as

$$-\mathcal{P}^{(\mathrm{i})} \equiv 4\pi \int_{\mathrm{r_i}}^{\mathrm{r_e}} (\boldsymbol{\Sigma} : \mathbf{D}^\star + \mathbf{M}\dot{:}\nabla\mathbf{D}^\star)\, \mathrm{r}^2 \mathrm{dr} \tag{57}$$

Using the expressions of the strain and gradient of the strain the relation (57) becomes

$$\begin{cases} -\mathcal{P}^{(\mathrm{i})} \equiv 4\pi \displaystyle\int_{\mathrm{r_i}}^{\mathrm{r_e}} \left[\Sigma_{\mathrm{rr}} \frac{\partial \mathrm{v}_\mathrm{r}^\star}{\partial \mathrm{r}} + 2\Sigma_{\theta\theta} \frac{\mathrm{v}_\mathrm{r}^\star}{\mathrm{r}} + 2M_{\theta\theta\mathrm{r}} \frac{\partial \left(\frac{\mathrm{v}_\mathrm{r}^\star}{\mathrm{r}}\right)}{\partial \mathrm{r}} \right] \mathrm{r}^2 \mathrm{dr} \\ \qquad + 4\pi \displaystyle\int_{\mathrm{r_i}}^{\mathrm{r_e}} \left[M_{\mathrm{rrr}} \frac{\partial^2 \mathrm{v}_\mathrm{r}^\star}{\partial \mathrm{r}^2} + M_{\mathrm{r}\theta\theta} \left(\frac{1}{\mathrm{r}} \frac{\partial \mathrm{v}_\mathrm{r}^\star}{\partial \mathrm{r}} - \frac{\mathrm{v}_\mathrm{r}^\star}{\mathrm{r}} \right) \right] \mathrm{r}^2 \mathrm{dr}. \end{cases}$$

After integration by parts, the expression (58) gives the formula

$$\begin{cases} -\mathcal{P}^{(\mathrm{i})} \equiv 4\pi \displaystyle\int_{\mathrm{r_i}}^{\mathrm{r_e}} \left[\frac{\partial \left(-\mathrm{r}^2 \Sigma_{\mathrm{rr}}\right)}{\partial \mathrm{r}} \mathrm{v}_r^\star + 2\mathrm{r}\Sigma_{\theta\theta} \mathrm{v}_\mathrm{r}^\star - 2 \frac{\partial \left(\mathrm{r}^2 M_{\theta\theta\mathrm{r}}\right)}{\partial \mathrm{r}} \frac{\mathrm{v}_\mathrm{r}^\star}{\mathrm{r}} \right] \mathrm{dr} \\ -4\pi \displaystyle\int_{\mathrm{r_i}}^{\mathrm{r_e}} \left[\frac{\partial \left(\mathrm{r}^2 M_{\mathrm{rrr}}\right)}{\partial \mathrm{r}} \frac{\partial \mathrm{v}_\mathrm{r}^\star}{\partial \mathrm{r}} + 4\mathrm{v}_\mathrm{r}^\star \frac{\partial \left(\mathrm{r} M_{\mathrm{r}\theta\theta}\right)}{\partial \mathrm{r}} + \mathrm{v}_\mathrm{r}^\star M_{\mathrm{r}\theta\theta} \right] \mathrm{dr} \\ +4\pi \left(\left[\mathrm{r}^2 \Sigma_{\mathrm{rr}} \mathrm{v}_\mathrm{r}^\star \right]_{\mathrm{r_i}}^{\mathrm{r_e}} + \left[\mathrm{r}^2 M_{\mathrm{rrr}} \frac{\partial \mathrm{v}_\mathrm{r}^\star}{\partial \mathrm{r}} \right]_{\mathrm{r_i}}^{\mathrm{r_e}} + \left[2\mathrm{r} M_{\theta\theta\mathrm{r}} \mathrm{v}_\mathrm{r}^\star \right]_{\mathrm{r_i}}^{\mathrm{r_e}} + \left[2\mathrm{r} M_{\mathrm{r}\theta\theta} \mathrm{v}_\mathrm{r}^\star \right]_{\mathrm{r_i}}^{\mathrm{r_e}} \right) \end{cases}$$

In Eq.(58), the operator $[]_{\mathrm{r_i}}^{\mathrm{r_e}}$ applied to any arbitrary function $\mathbf{X}$ represents the difference $\mathbf{X}(\mathrm{r_i}) - \mathbf{X}(\mathrm{r_e})$. After development, Eq.(58) yields

$$\begin{cases} -\mathcal{P}^{(\mathrm{i})} \equiv 4\pi \displaystyle\int_{\mathrm{r_i}}^{\mathrm{r_e}} \left[-2\mathrm{r}\Sigma_{\mathrm{rr}} - r^2 \frac{\partial \Sigma_{\mathrm{rr}}}{\partial \mathrm{r}} + 2\mathrm{r}\Sigma_{\theta\theta} + \mathrm{r}^2 \frac{\partial^2 M_{\mathrm{rrr}}}{\partial \mathrm{r}^2} + 4\mathrm{r} \frac{\partial M_{\mathrm{rrr}}}{\partial \mathrm{r}} \right] \mathrm{v}_\mathrm{r}^\star \mathrm{dr} \\ +4\pi \displaystyle\int_{\mathrm{r_i}}^{\mathrm{r_e}} \left[-4M_{\theta\theta\mathrm{r}} - 2\mathrm{r} \frac{\partial M_{\theta\theta\mathrm{r}}}{\partial \mathrm{r}} - 8\mathrm{M}_{\mathrm{r}\theta\theta} - 4\mathrm{r} \frac{\partial M_{\mathrm{r}\theta\theta}}{\partial \mathrm{r}} + 2M_{\mathrm{rrr}} \right] \mathrm{v}_\mathrm{r}^\star \mathrm{dr} \\ +4\pi \left[\left(\mathrm{r}^2 \Sigma_{\mathrm{rr}} - \frac{\partial \left(\mathrm{r}^2 \mathrm{M}_{\mathrm{rrr}}\right)}{\partial \mathrm{r}} + 2r M_{\theta\theta\mathrm{r}} + 4\mathrm{r} M_{\mathrm{r}\theta\theta} \right) \mathrm{v}_\mathrm{r}^\star + \mathrm{r}^2 M_{\mathrm{rrr}} \frac{\partial \mathrm{v}_\mathrm{r}^\star}{\partial \mathrm{r}} \right]_{\mathrm{r_i}}^{\mathrm{r_e}}. \end{cases}$$

The application of the principle of virtual work (with the virtual power of external forces $\mathcal{P}^{(\mathrm{e})} = 4\pi \mathrm{b}^2 \mathrm{T} \mathrm{v}_\mathrm{b}^\star$ where T is a traction force applied on the outer surface of the hollow sphere) gives the balance equations

$$\begin{aligned} \frac{\partial \Sigma_{\mathrm{rr}}}{\partial \mathrm{r}} + \frac{2}{\mathrm{r}} (\Sigma_{\mathrm{rr}} - \Sigma_{\theta\theta}) - \frac{\partial^2 M_{\mathrm{rrr}}}{\partial \mathrm{r}^2} - \frac{4}{\mathrm{r}} \frac{\partial M_{\mathrm{rrr}}}{\partial \mathrm{r}} - \frac{2}{\mathrm{r}^2} M_{\mathrm{rrr}} + \frac{2}{\mathrm{r}^2} \frac{\partial M_{\theta\theta\mathrm{r}}}{\partial \mathrm{r}} \\ + \frac{4}{\mathrm{r}^2} M_{\theta\theta\mathrm{r}} + \frac{4}{\mathrm{r}} \frac{\partial M_{\mathrm{r}\theta\mathrm{\theta}}}{\partial \mathrm{r}} + \frac{8}{\mathrm{r}^2} M_{\mathrm{r}\theta\theta} = 0. \end{aligned} \tag{58}$$

and the boundary conditions

$$\begin{cases} \mathrm{r}^2 \Sigma_{\mathrm{rr}} - \dfrac{\partial \left(\mathrm{r}^2 M_{\mathrm{rrr}} \right)}{\partial \mathrm{r}} + 2\mathrm{r} M_{\theta\theta\mathrm{r}} + 4\mathrm{r} M_{\mathrm{r}\theta\theta} = 0 \quad \text{for} \quad \mathrm{r} = \mathrm{r_i} \quad \text{and} \quad \mathrm{r} = \mathrm{r_e} \\ M_{\mathrm{rrr}} = 0 \quad \text{for} \quad \mathrm{r} = \mathrm{r_i} \quad \text{and} \quad \mathrm{r} = \mathrm{r_e} \end{cases} \tag{59}$$